

# DIFFRACTIVE DISSOCIATION IN THE INTERACTING GLUON MODEL

F.O. Durães<sup>1\*</sup>, F.S. Navarra<sup>1,2†</sup> and G. Wilk<sup>2‡</sup>

<sup>1</sup>*Instituto de Física, Universidade de São Paulo  
C.P. 66318, 05389-970 São Paulo, SP, Brazil*

<sup>2</sup>*Soltan Institute for Nuclear Studies, Nuclear Theory Department  
ul. Hoża 69, Warsaw, Poland*

July 4, 2018

## Abstract

We have extended the Interacting Gluon Model (IGM) to calculate diffractive mass spectra generated in hadronic collisions. We show that it is possible to treat both diffractive and non-diffractive events on the same footing, in terms of gluon-gluon collisions. A systematic analysis of available data is performed. The energy dependence of diffractive mass spectra is addressed. They show a moderate narrowing at increasing energies. Predictions for LHC energies are presented.

PACS number(s): 13.85.Qk, 11.55.Jy

---

\*e-mail: dunga@uspif.if.usp.br

†e-mail: navarra@uspif.if.usp.br

‡e-mail: wilk@fuw.edu.pl

# 1 Introduction

In the last years, diffractive scattering processes have received increasing attention for several reasons. These processes may, for example, explain many features of particle production and, in particular, heavy flavour production [1] and Centauro events [2]. They are also related to the large rapidity gap physics and the structure of the Pomeron [3]. In a diffractive scattering, one of the incoming hadrons emerges from the collision only slightly deflected and there is a large rapidity gap between it and the other final state particles resulted from the other excited hadron. In some models diffraction is due to the Pomeron exchange but the exact nature of the Pomeron in QCD is not elucidated yet. The first test of a theory (or a model) of diffractive dissociation (DD) is the ability to properly describe the mass ( $M_X$ ) distribution of diffractive systems, which has been measured in many experiments [4] and parametrized as  $(M_X^2)^{-\alpha}$  with  $\alpha \simeq 1$ . Data presented in [4] were taken at the Tevatron collider ( $\sqrt{s} = 1.8$  TeV). They allow us to make comparison with CERN [5] lower energies data and observe the energy dependence of the mass spectrum. In the old Regge theory, the assumption of Pomeron dominance implies that the mass spectrum behaves like  $1/M_X^2$  and does not depend on the energy [6] whereas in [4] a slight deviation from this behaviour was reported.

In this work we intend to study diffractive mass distributions using the Interacting Gluon Model (IGM) developed by us recently [7, 8, 9]. In particular, we are interested in the energy dependence of these distributions and their connection with inelasticity distributions [10, 8]. One advantage of the IGM is that it was designed in such a way that the energy-momentum conservation is taken care of before all other dynamical aspects. This feature makes it very appropriate for the study of energy flow in high energy hadronic and nuclear reactions [7, 8, 9] and in cosmic ray studies [10]. In particular, as shown in [8, 9], the IGM was very useful in analysing data and making predictions on the behaviour of inelasticities and leading particle spectra, including leading charm production [11]. The aim of the present work is to demonstrate that the main characteristics of the DD processes mentioned above emerge naturally from the standard IGM, enlarging profoundly its range of applications.

In the following section we present for readers convenience the basic elements of the IGM. It is then applied to DD processes in Section 3 where we also carefully explain what DD means in terms of the IGM and how it differs from the conventional Regge Pomeron approach. Section 4 contains our numerical results and comparison with data and the last section is devoted to our conclusions.

# 2 Interacting Gluon Model

## 2.1 General ideas

The Interacting Gluon Model is based on the following idea [12] : since about half of a hadron momentum is carried by gluons and since gluons interact more strongly than quarks, during a collision there is a separation of constituents. Valence quarks tend to be fast forming leading particles whereas gluons tend to be stopped in the central rapidity region. This picture is consistent with string formation and fragmentation as it is formulated in the Lund Model or in the Dual Parton Model. These models are based on the concept of string and were constructed to work at low average transverse momenta. When, in the late eighties, the energy of hadronic collisions increased by more than one order of magnitude it became necessary to incorporate the concept of parton and of hard and semi-hard collisions. The latter are collisions between partons at a moderate scale ( $Q^2 \simeq (2 \text{ GeV})^2$ ) which however still allows for the use of perturbative QCD. The scattered partons form the so-called minijets. At  $\sqrt{s} = 540$  GeV the minijet cross section is already 25% of the total inelastic cross section. A new generation of models appeared using the concept of parton and the QCD parton model formalism and trying to understand

minimum-bias multiparticle physics extending the parton model to semihard (moderate) energy scales. Among these models we mention those presented by Gaisser and Stanev [13], Sjostrand [14], Wang [15] and Geiger [16]. The IGM belongs to this class of models. In all these models one finds at a certain point expresssions of the type

$$\int_{Q^2}^1 dx_1 \int_{\frac{Q^2}{x_1}}^1 dx_2 f(x_1, Q^2) f(x_2, Q^2) \sigma(x_1, x_2, Q^2) \quad (1)$$

where  $f$  and  $\sigma$  are parton momentum distribution and parton-parton elementary cross section respectively.  $Q^2$  is the scale. Apart from some ambiguity in choosing the scale, these models have to face the problem that even at very high energies a significant part of a hadronic collision occurs at scales lower than the semihard one. At this point  $f$  and  $\sigma$  are not very well known. The atitude taken in HIJING [15], in the Parton Cascade Model [16] and also in the IGM is to extrapolate these quantities to lower scales. These extrapolations can be continuously improved, especially in view of the advance of our knowledge on non-perturbative effects. There are, for example, models for distribution functions which work at scales as low as  $0.3 \text{ GeV}^2$  [17]. As for  $\sigma$  one can compute non-perturbative effects in the context of an operator product expansion [18]. Inspite of these limitations these models have the advantage of dealing with partons and being thus prepared to incorporate perturbative QCD in a natural way. This is welcome since perturbative processes are expected to be increasingly important at higher energies. Compared to the other models mentioned above, the IGM is simpler because it is designed to study energy flow and makes no attempt to calculate cross sections or to follow hadronization in great detail. This simplifies the calculations and avoids time consuming numerical simulations. The most important aspect of the IGM, shared with those models, is the assumption of multiple parton-parton incoherent scattering which is implicit in the Poissonian distribution of the number of parton-parton collisions (which is also used in refs. [14, 13, 15]) used below. In going to lower resolution scales this independent collision approximation becomes questionable. On the other hand lattice QCD calculations [19] in the strong coupling regime indicate that the typical correlation length of the soft gluon fields is around 0.2 fm. This is still smaller than the typical hadronic size. Therefore the independent collision approximation may still be a reasonable one. From the practical point of view, it was shown in [7] that replacing the Poissonian distribution by a broader one does not affect the results significantly as long as some mass scale is introduced to cut off the very low  $x$  region.

## 2.2 Formulation of the model

The IGM is based on the assumed dominance of hadronic collisions by gluonic interactions [12] and can be summarized as follows [7] (cf. Fig. 1a):

- (i) The two colliding hadrons are represented by valence quarks carrying their quantum numbers (charges) plus the accompanying clouds of gluons (which represent also the sea  $q\bar{q}$  pairs and therefore should be regarded as effective ones).
- (ii) In the course of a collision gluonic clouds interact strongly and form a gluonic *central fireball* (CF) located in the central region of the reaction.
- (iii) The valence quarks (plus those gluons which did not interact) get excited and form *leading jets* (LJ's) (or *beam jets*) which then populate mainly the fragmentation regions of the reaction.

It should be stressed that the IGM has been formulated originally in order to give the initial conditions for hydrodynamical models by providing in a dynamical way the so called *inelasticity* of the reaction understood usually as the (invariant) fraction of energy stored in the CF:

$$K = \sqrt{x \cdot y} \quad (2)$$

with  $x$  and  $y$  being the fractions of the initial energy-momenta of the respective projectiles allocated to the CF. This variable and, in particular, its energy dependence is of vital importance in cosmic ray studies as it is the necessary ingredient allowing to deduce any elementary information from cosmic ray experiments [10].

According to the IGM, pairs of gluons collide and form “minifireballs” (MF’s). In collisions at higher scales a minifireball is the same as a pair of minijets or jets. In the study of energy flow the details of fragmentation and hadron production are not important. Most of the MF’s will be in the central region and we assume that they coalesce forming the CF. The probability to form a fireball carrying momentum fractions  $x$  and  $y$  of two colliding hadrons is defined as the sum over (an undefined number  $n$  of) MF’s [7]:

$$\chi(x, y) = \sum_{\{n_i\}} \delta \left( x - \sum_i n_i x_i \right) \delta \left( y - \sum_i n_i y_i \right) \prod_{\{n_i\}} P(n_i) \quad (3)$$

(all masses and transverse momenta are neglected in what follows). The distribution of the number of MF’s is given by  $P(n_i)$  for which we use Poisson distributions:

$$P(n_i) = \frac{(\bar{n}_i)^{n_i} \exp(-\bar{n}_i)}{n_i} \quad (4)$$

corresponding to independent production. Expressing the delta functions via Fourier integrals one can perform all summations, transform certain summations over  $\bar{n}_i$  into integrals and make the replacement  $d\bar{n}_i/dxdy = \omega(x, y)$  arriving at the general formula [7]:

$$\begin{aligned} \chi(x, y) &= \frac{\chi_0}{2\pi\sqrt{D_{xy}}} \cdot \\ &\cdot \exp \left\{ -\frac{1}{2D_{xy}} [\langle y^2 \rangle (x - \langle x \rangle)^2 + \langle x^2 \rangle (y - \langle y \rangle)^2 - 2\langle xy \rangle (x - \langle x \rangle)(y - \langle y \rangle)] \right\}, \end{aligned} \quad (5)$$

where

$$D_{xy} = \langle x^2 \rangle \langle y^2 \rangle - \langle xy \rangle^2$$

and

$$\langle x^n y^m \rangle = \int_0^1 dx x^n \int_0^1 dy y^m \omega(x, y), \quad (6)$$

with  $\chi_0$  being a normalization factor defined by the condition that

$$\int_0^1 dx \int_0^1 dy \chi(x, y) \Theta(xy - K_{min}^2) = 1 \quad (7)$$

with  $K_{min} = \frac{m_0}{\sqrt{s}}$  being the minimal inelasticity defined by the mass  $m_0$  of the lightest possible CF. The, so called, spectral function  $\omega(x, y)$  contains all the dynamical input of the IGM in the general form of (cf. [9])

$$\omega(x, y) = \frac{\sigma_{gg}(xys)}{\sigma(s)} G(x) G(y) \Theta(xy - K_{min}^2), \quad (8)$$

where  $G$ ’s denote the effective number of gluons from the corresponding projectiles (approximated by the respective gluonic structure functions) and  $\sigma_{gg}$  and  $\sigma$  the gluonic and hadronic cross sections, respectively. These are basic formulae of the IGM from which all its applications are derived [20].

### 3 Diffractive Dissociation in the IGM approach

It is now quite straightforward to extend the IGM also to diffractive dissociation processes. In Fig. 1b we show schematically the IGM picture of a diffractive dissociation event. Unlike in Fig. 1a here only one of

the protons loses fraction  $x$  of its original momentum and gets excited forming a LJ carrying  $x_L = 1 - x$  fraction of the initial momentum. The other one, which we shall call here the diffracted proton, loses only a fraction  $y$  of its momentum but otherwise remains intact [25]. In the standard IGM presented in the previous section we were computing the probability  $\chi(x, y)$  of depositing energy fractions  $x$  and  $y$  in the central region in the form of gluonic CF of mass  $M = \sqrt{xy s}$ , which subsequently was decaying and producing particles. Here we shall be rather interested in the mass  $M_X$ , a new variable in our problem, which, as can be seen in Fig. 1b, is just the invariant mass of a system composed of the CF and the leading jet formed by one of the colliding protons (we shall call it also *diffractive mass*). Denoting by  $E_L$  and  $P_L$  the energy and momentum of the upper (in Fig. 1b) proton and by  $W$  and  $P$  the energy and momentum of the CF,

$$P_L = E_L = \frac{\sqrt{s}}{2} (1 - x), \quad P = \frac{\sqrt{s}}{2} (x - y), \quad W = \frac{\sqrt{s}}{2} (x + y), \quad (9)$$

the energy  $E_X$  and momentum  $P_X$  of the diffractive cluster are given by:

$$E_X = E_L + W = \frac{\sqrt{s}}{2} (1 + y) \quad \text{and} \quad P_X = P_L + P = \frac{\sqrt{s}}{2} (1 - y) \quad (10)$$

leading to the following expressions for the mass of our diffractive cluster,  $M_X$ , and its rapidity,  $Y_X$ :

$$M_X = \sqrt{E_X^2 - P_X^2} = \sqrt{s \cdot y}, \quad (11)$$

$$Y_X = \frac{1}{2} \ln \frac{E_X + P_X}{E_X - P_X} = \frac{1}{2} \ln \frac{1}{y}, \quad (12)$$

where  $\sqrt{s}$  is the invariant energy of the  $pp$  system. We are working in the cm frame of the incoming nucleons. All masses have been neglected [26].

In the limit  $y \rightarrow 1$ , the whole available energy is stored in  $M_X$  which remains then at rest, i.e.,  $Y_X = 0$ . For small values of  $y$  we have small masses  $M_X$  located at large rapidities  $Y_X$ . In order to regard our process as being trully of the DD type we must assume that all gluons from the target proton participating in the collision (i.e., those emitted from the lower vertex in Fig. 1b) *have to form a colour singlet*. Only then a large rapidity gap will form separating the diffracted proton (in the lower part of our Fig. 1) and the  $M_X$  system (in its upper part), which is the experimental requirement defining a diffractive event. Otherwise a colour string would develop, connecting the diffracted proton and the diffractive cluster, and would eventually decay, filling the rapidity gap with produced secondaries. In this way we are effectively introducing an object resembling closely (but by no means identical to) what is known as Pomeron ( $\mathcal{P}$ ) and therefore in what follows we shall use this notion as a handy abbreviation of notation [27]. The probability of finding the “bunch” of gluons (that forms the Pomeron) mentioned above in a colour singlet configuration is not computable at a more fundamental level because the model is simple and does not involve colour quantum numbers explicitly. However this probability is represented indirectly in the cross section between the gluonic bunch and the other proton, the parameter  $\sigma$  discussed below in eq. (18).

In our approach the definition of the object  $\mathcal{P}$  is essentially only kinematical [30], very much in the spirit of those used in all other works which deal with diffractive processes in the parton and/or string language [31, 32, 33, 34]. We shall therefore try to derive the whole  $M_X^2$  dependence directly from the IGM. Our first step necessary to adapt the standard IGM to DD collisions will be the introduction a kinematical restriction in the formula for the moments eq.(6) preventing gluons coming from the diffracted proton (and forming our object  $\mathcal{P}$ ) to carry more energy than the one released in the diffractive system. Therefore we shall write it as

$$\langle x^n y^m \rangle = \int_0^1 dx x^n \int_0^{y_{max}} dy y^m \omega(x, y), \quad (13)$$

where  $y_{max} = \frac{M_X^2}{s}$  and the meaning of the spectral function  $\omega(x, y)$  remains the same as before.

We can now calculate the diffractive mass distribution  $M_X$  using the  $\chi(x, y)$  function by simply performing a change of variables (cf. eq.(11)),

$$\begin{aligned} \frac{dN}{dM_X^2} &= \int_0^1 dx \int_0^1 dy \chi(x, y) \delta(M_X^2 - sy) \Theta(xy - K_{min}^2) \\ &= \frac{1}{s} \int_{\frac{m_0^2}{M_X^2}}^1 dx \chi\left(x, \frac{M_X^2}{s}\right), \end{aligned} \quad (14)$$

In the IGM [7, 9] the distribution  $\chi(x, y)$  is a wide gaussian in the variables  $x$  and  $y$  changing slowly with the energy  $\sqrt{s}$ . Substituting now eq.(5) into eq.(14) we arrive at the following simple expression for the diffractive mass distribution:

$$\frac{dN}{dM_X^2} = \frac{1}{s} \cdot F(M_X^2, s) \cdot H(M_X^2, s) \quad (15)$$

where

$$F(M_X^2, s) = \exp\left[-\frac{\langle x^2 \rangle}{2D_{xy}} \left(\frac{M_X^2}{s} - \langle y \rangle\right)^2\right] \quad (16)$$

and

$$\begin{aligned} H(M_X^2, s) &= \frac{\chi_0}{2\pi\sqrt{D_{xy}}} \int_{\frac{m_0^2}{M_X^2}}^1 dx \cdot \\ &\cdot \exp\left\{-\frac{1}{2D_{xy}} \left[\langle y^2 \rangle(x - \langle x \rangle)^2 - 2\langle xy \rangle(x - \langle x \rangle) \left(\frac{M_X^2}{s} - \langle y \rangle\right)\right]\right\}. \end{aligned} \quad (17)$$

The moments  $\langle q^n \rangle$ ,  $q = x, y$  and  $n = 1, 2$  are given by (13) and are the only place where dynamical quantities like the gluonic and hadronic cross sections appear in the IGM. At this point we emphasize that we are all the time dealing with a proton- proton scattering. However, as was said above, we are in fact selecting a special class of events and therefore we must choose the correct dynamical inputs in the present situation, specially the gluon distribution inside the diffracted proton and the hadronic cross section  $\sigma$  appearing in  $\omega$ . As a first approximation we shall take  $G^P(y) = G^p(y) = G(y)$  (cf. [28]), with  $G(x) = p(m+1) \frac{(1-y)^m}{y}$ , with  $m=5$ , the same already used by us before [9]. The amount of the diffracted nucleon momentum,  $p$ , allocated specifically to the  $\mathcal{IP}$  gluonic cluster and the hadronic cross section  $\sigma$  are both unknown. However, they always appear as a ratio  $(\frac{p}{\sigma})$  of parameters in  $\omega$  and different choices are possible. Just in order to make contact with the present knowledge about the Pomeron, we shall choose

$$\sigma(s) = \sigma^{PP} = a + b \ln \frac{s}{s_0} \quad (18)$$

where  $s_0 = 1 \text{ GeV}^2$  and  $a$  and  $b$  are parameters to be fixed from data analysis. As it will be seen,  $\sigma(s)$  turns out to be a very slowly varying function of  $\sqrt{s}$  assuming values between 2.6 and 3.0 mb, which is a well accepted value for the Pomeron-proton cross section, and  $p \simeq 0.05$ .

Before performing a full numerical calculation let us estimate eqs.(15) and (17) keeping only the most singular parts of the gluonic distributions used (i.e.,  $G(x) \simeq 1/x$ ) and collecting all other factors in eq.(8) in a single parameter  $c$ . Let us first assume that the ratio of the cross sections  $\frac{\sigma(xys)}{\sigma(s)}$  does not depend on  $x$  and  $y$ . Neglecting all terms of the order of  $\frac{m_0^2}{s}$  and  $\frac{m_0^2}{M_X^2}$  we arrive at the following expressions for the moments calculated in eq.(13):

$$\langle x \rangle = 2 \langle x^2 \rangle \simeq c \cdot \ln \frac{M_X^2}{m_0^2}; \quad (19)$$

$$\langle y \rangle = 2 \frac{s}{M_X^2} \langle y^2 \rangle \simeq c \cdot \frac{M_X^2}{s} \cdot \ln \frac{M_X^2}{m_0^2}; \quad (20)$$

$$\langle x \cdot y \rangle \simeq c \left( \frac{M_X^2}{s} - \frac{m_0^2}{s} \cdot \ln \frac{M_X^2}{m_0^2} \right). \quad (21)$$

Notice that in all cases of interest  $\langle x \cdot y \rangle$  is much smaller than other moments (by a factor  $\ln \frac{M_X^2}{m_0^2}$ , at least). It means that  $D_{xy} \simeq \langle x^2 \rangle \langle y^2 \rangle$  and consequently

$$\begin{aligned} F(M_X^2, s) &\simeq \exp \left[ -\frac{\left( \frac{M_X^2}{s} - \langle y \rangle \right)^2}{2 \langle y^2 \rangle} \right] \\ &\simeq \exp \left[ -\frac{\left( 1 - c \cdot \ln \frac{M_X^2}{m_0^2} \right)^2}{c \cdot \ln \frac{M_X^2}{m_0^2}} \right] \end{aligned} \quad (22)$$

and

$$\begin{aligned} H(M_X^2, s) &\simeq \frac{\chi_0}{2\pi\sqrt{D_{xy}}} \int_{\frac{m_0^2}{M_X^2}}^1 dx \exp \left[ -\frac{(x - \langle x \rangle)^2}{2\langle x^2 \rangle} \right] \simeq \text{const} \cdot \frac{\sqrt{\langle x^2 \rangle}}{\sqrt{D_{xy}}} = \text{const} \cdot \frac{1}{\sqrt{\langle y^2 \rangle}} \\ &\simeq \text{const} \cdot \frac{s}{M_X^2 \cdot \sqrt{c \cdot \ln \frac{M_X^2}{m_0^2}}} \end{aligned} \quad (23)$$

leading to

$$\begin{aligned} \frac{dN}{dM_X^2} &\simeq \frac{1}{s} \cdot H(M_X^2, s) \cdot F(M_X^2, s) \\ &\simeq \frac{\text{const}}{M_X^2} \cdot \frac{1}{\sqrt{c \cdot \ln \frac{M_X^2}{m_0^2}}} \cdot \exp \left[ -\frac{\left( 1 - c \cdot \ln \frac{M_X^2}{m_0^2} \right)^2}{c \cdot \ln \frac{M_X^2}{m_0^2}} \right]. \end{aligned} \quad (24)$$

The expression above is governed by the  $\frac{1}{M_X^2}$  term. The other two terms have a weaker dependence on  $M_X^2$ . They distort the main  $(\frac{1}{M_X^2})$  curve in opposite directions and tend to compensate each other. It is therefore very interesting to note that even before choosing a very detailed form for the gluon distributions and hadronic cross sections we obtain analytically the typical shape of a diffractive spectrum.

## 4 Comparison with experimental data

In Fig. 2a we show our diffractive mass spectrum and compare it to experimental data from the CERN-ISR [35], which are usually parametrized by the form  $\frac{1}{M_X^2}$ . These spectra were calculated with expression (15) with the same gluon distributions, cross sections and the mass parameter  $m_0$  ( $m_0 = 350$  MeV) used in previous works [7, 8, 9]. As it can be seen, the agreement between our curves and data is reasonable. At large values of  $\frac{M_X^2}{s}$ , experimental points start to flatten out, deviating from the  $\frac{1}{M_X^2}$  behaviour. This may be due to the contribution of non-diffractive events. We expect therefore some discrepancy between theory and experiment in this region. At very low values of  $\frac{M_X^2}{s}$  and lower energies  $\sqrt{s}$  our model does not give a good description of data. Here again some discrepancy should be expected because we are neglecting all resonance effects. In principle a better agreement between theory and data could be achieved in this region. It would be enough to choose  $m_0 = 550$  MeV keeping everything else as before. The result is shown in Fig. 2b. A discrepancy persists at very low masses at the lowest center of mass energy  $\sqrt{s}$ . However this region is almost beyond the validity domain of the model. Instead of changing  $m_0$  (which would also require a change in our previous works), we prefer to keep its usual value. Given the qualitative nature of the present work, we choose to be consistent with our previous works in prejudice of the quality of the fits.

Fig.3 and 4 show similar comparisons for  $\sqrt{s} = 546$  and 1800 GeV respectively. Data are from refs. [5] and [4]. Again we find reasonable agreement with experiment. In the low  $\frac{M_X^2}{s}$  region at higher  $\sqrt{s}$  the agreement is very good. All the curves above were obtained with  $a = 2.6$  mb and  $b = 0.01$  mb.

As a straightforward extension of our calculation we now apply expression (15) to the study of diffractive pion-proton and kaon-proton scattering. We first consider the cases  $p + \pi \rightarrow p + X$  and  $p + K \rightarrow p + X$ . This corresponds to replace the proton by a pion or a kaon in the upper line of Fig. 1b, everything else remaining the same. We must also substitute the gluon distributions in the proton,  $G(x)$ , by the corresponding gluon distributions in the pion and kaon, taken from [36]. Here, for simplicity, we take  $G^\pi(x) = G^K(x)$ . This is supported by an ACCMOR collaboration data analysis [37]. We also assume that  $\sigma^{Pp} = \sigma^{P\pi} = \sigma^{PK}$ . The comparison between our results and data from the EHS/NA22 collaboration [38] is shown in Figs. 5a (pions) and 5b (kaons). We may also have diffracted mesons, which undergo reactions of the type  $\pi + p \rightarrow \pi + X$  and  $K + p \rightarrow K + X$ . This corresponds to replace the proton by a pion or a kaon in the lower line of Fig. 1b, substituting also the corresponding gluon distributions. The comparison between our results and experimental data [38] is shown in Fig. 6a (pions) and 6b (kaons). As it can be seen, a good description of data is obtained.

Let us consider now the energy dependence of our results. The CDF collaboration studied single diffractive events and found some energy dependence in the diffractive mass spectrum. This fact is illustrated by writing

$$\frac{s}{\sigma_{SD}} \frac{d\sigma_{SD}}{dM_X^2} \propto \frac{1}{(M_X^2)^{1+\epsilon}} \quad (25)$$

where the factor  $\epsilon$  which has been reported to be [39]  $\epsilon = 0.121 \pm 0.011$  at  $\sqrt{s} = 546$  GeV and  $\epsilon = 0.103 \pm 0.017$  at  $\sqrt{s} = 1800$  GeV, respectively. Considering the error bars one might say that this value is just constant (and that there would be no indication of energy dependence), but a real (albeit small one) change in  $\epsilon$  is not excluded. Therefore, if confirmed, it would mean that the distribution becomes slightly broader.

In the IGM everything is from the beginning energy dependent and so should be the diffractive mass distribution. We start analysing the analytical approximation eqs. (15,22, 23). In (23) we see that the  $s$ -dependence factorizes and the function  $H(M_X^2)$  has the same shape for all energies, the difference being only a multiplying factor (in numerical calculations this behaviour is slightly violated). In (22) the  $s$ -dependence does not factorize and remains in the moments or, equivalently, in the variable  $c \cdot F(M_X^2)$  is a broad function with maximum value determined by the moment  $\langle y \rangle$  which increases with the energy, making  $F$  to "rotate" in a way that it becomes higher at lower values of  $M_X^2$  and becomes deeper at larger values of  $M_X^2$ . When we multiply  $H$  (which goes essentially like  $1/M_X^2$ ) by  $F$  it becomes steeper. This behaviour of  $F$  and  $H$  is illustrated in Fig. 7a and 7b respectively, which show the numerical evaluation of eqs. (16) and (17). The result of the numerical evaluation of eq. (15) is presented in Fig. 8. There we show the energy dependence of our diffractive mass spectra in proton-proton scattering. Fig. 8a shows diffractive mass spectra for  $\sqrt{s} = 23.5$  GeV (solid lines), 44.6 GeV (dashed lines) and 62.4 GeV (dotted lines). Fig. 8b shows spectra at  $\sqrt{s} = 0.54$  TeV (solid lines), 0.9 TeV (dashed lines) and 1.8 TeV (dotted lines). Finally Fig. 8c shows our prediction for the diffractive mass spectrum at LHC ( $\sqrt{s} = 14$  TeV) compared to the Tevatron one. The spectra in Fig. 8a and 8b are the same of Figs. 2, 3 and 4. It is interesting to note that the behaviour that we find is not in contradiction with data. In all curves we observe a modest narrowing as the energy increases. This small effect means that the diffractive mass becomes a smaller fraction of the available energy  $\sqrt{s}$ . In other words, the "diffractive inelasticity" decreases with energy and consequently the "diffracted leading particles" follow a harder  $x_F$  spectrum. Physically, in the context of the IGM, this means that the deposited energy is increasing with  $\sqrt{s}$  but it will be mostly released outside the phase space region that we are selecting. A measure of the "diffractive inelasticity" is the quantity  $\xi = \frac{M_X^2}{s}$ . Making a trivial change of variables in eq.(15) we can calculate its average value  $\langle \xi \rangle$  :

$$\langle \xi \rangle (s) = \int_{\xi_{min}}^{\xi_{max}} d\xi \frac{dN}{d\xi} \xi \quad (26)$$

where  $\xi_{min}$  ( $= \frac{1.5}{s}$ ) and  $\xi_{max}$  ( $= 0.1$ ) are the same used in ([39]) for the purpose of comparison. In Fig. 9 we plot  $\langle \xi \rangle$  against  $\sqrt{s}$ . As it can be seen  $\langle \xi \rangle$  decreases with  $\sqrt{s}$  not only because  $\xi_{min}$  becomes smaller but also because  $\frac{dN}{d\xi}$  changes with the energy, falling faster. This qualitative behaviour of  $\langle \xi \rangle$  is in agreement with the estimate of the same quantity extracted from cosmic ray data analysis [40]. Also shown in Fig. 9 is the quantity  $\langle \xi^\varepsilon \rangle$  (which has been discussed in [39] in connection with the energy dependence of the single diffractive cross-section) for  $\varepsilon = 0.08$  (dashed lines) and  $\varepsilon = 0.112$  (dotted lines).

The energy behaviour of  $\frac{dN}{dM_X^2}$  is determined by the moments (13) and (8). Since  $\sigma_{gg}(s)$  and  $G(x)$  are the same as in previous works, being thus fixed, the only source of uncertainty in the  $s$ -dependence of the results is in the ratio  $\frac{p}{\sigma}$ , which is the only free parameter in the model. All curves presented above were obtained with the choice (18) made for  $\sigma$  and with  $p \simeq 0.05$ . We have checked that for a stronger growth of  $\sigma^{PP}$  with  $\sqrt{s}$  the energy behaviour of  $\frac{dN}{dM_X^2}$  might become even the opposite of the one found here, i.e., the diffractive mass distribution would become broader at higher energies. However these strongly  $s$ -dependent parametrizations do not give an acceptable description of the existing data and were therefore excluded. Considering what was said above one might think that we can discriminate between different Pomeron-proton cross sections and we could use this model to extract  $\sigma^{PP}$  from data. We stress however that, in this model, only the ratio  $\frac{p}{\sigma}$  enters effectively in the calculations and it is impossible to completely disentangle these two variables. In this sense, the almost constancy (with  $\sqrt{s}$ ) of  $\sigma^{PP}$  may be just an indication of some increase of  $p$  with  $\sqrt{s}$  in a way that the ratio  $\frac{p}{\sigma}$  "scales" with the energy.

## 5 Conclusions

To conclude, we have shown that:

- (i) The original IGM ([7, 8, 9]) is reasonably successful in describing non-diffractive events. With only two natural changes, namely the introduction of the kinematical cut-off  $y_{max} = \frac{M_X^2}{s}$  and the multiplication of the function  $\omega$  by a constant factor reflecting the essentially unknown combination of  $IP$ -proton cross section  $\sigma$  and the amount of gluonic energy-momentum of the diffractive proton allocated to the object  $IP$ ,  $p$  (in form of the ratio  $\frac{p}{\sigma}$ ), (with all other parameters kept as in previous applications of IGM) it turns out to be also able to provide a reasonable description of diffractive events [41] and their energy dependence. We predict that, at higher energies, a narrowing of the  $M_X^2$  distribution may be observed.
- (ii) As is obvious from Fig. 1b, it provides a detailed description of the diffractive cluster (of mass  $M_X$ ), *disentangling* it in a natural way into gluonic cluster of mass  $M$  containing the majority of produced secondaries (which corresponds to CF in the original IGM) and leading jet (inside the diffractive system) with momentum fraction  $x_L$  carrying quantum numbers of the diffractively excited projectile. This fact may be very usefull for the cosmic ray applications of the IGM, in particular to studies using DD like those presented in [2, 42] (where such disentanglement seems to be important and so far was introduced in an *ad hoc* way only).

Acknowledgements: This work has been supported by FAPESP, CNPQ (Brazil) and KBN (Poland). F.S.N. is deeply indepted to his Polish colleagues from SINS, Warsaw, for the hospitality extended to him during his stay there. We would like to warmly thank R. Covolan and Y. Hama for many fruitful discussions.

## References

- [1] M. Heyssler, "Diffractive Heavy Flavour Production at the Tevatron and the LHC", hep-ph/9602420; A. Bialas and W. Szeremeta, *Phys. Lett.* **B296** (1992) 191; K. Eggert et al. (UA1 Collab.), *Search for diffractive heavy flavour production at the CERN proton-antiproton collider*, in: *Elastic and diffractive scattering*, ed. K. Goulianos, Ed. Frontière, Gif-sur-Yvette, 1988.
- [2] R. Attalah and J.N. Capdevielle, *J. Phys.* **G19** (1993) 1381.
- [3] J.D. Bjorken, *Nucl. Phys. (Proc. Suppl.)* **B25** (1992) 253.
- [4] N.A. Amos et al. (E710 Collab.), *Phys. Lett.* **B301** (1993) 313; F. Abe et al. (CDF Collab.), *Phys. Rev.* **D50** (1994) 5535 (and references therein).
- [5] M. Bozzo et al. (UA4 Collab.), *Phys. Lett.* **B136** (1984) 217.
- [6] K. Goulianos, *Phys. Rep.* **101** (1983) 169.
- [7] G.N. Fowler, F.S. Navarra, M. Plümer, A. Vourdas, R.M. Weiner and G. Wilk, *Phys. Rev.* **C40** (1989) 1219; G. Fowler, R.M. Weiner and G. Wilk, *Phys. Rev. Lett.* (1985) 173; G.N. Fowler, A. Vourdas, R.M. Weiner and G. Wilk, *Phys. Rev.* **D35** (1987) 870;
- [8] F.O. Durães, F.S. Navarra and G. Wilk, *Phys. Rev.* **D50** (1994) 6804 and references therein.
- [9] F.O. Durães, F.S. Navarra and G. Wilk, *Phys. Rev.* **D47** (1993) 3049.
- [10] Yu.A. Shabelski, R.M. Weiner, G. Wilk and Z. Włodarczyk, *J. Phys.* **G18** (1992) 1281; Z. Włodarczyk, *J. Phys.* **G21** (1995) 281.
- [11] F.O. Durães, F.S. Navarra, C.A.A. Nunes and G. Wilk, *Phys. Rev.* **D53** (1996) 6136.
- [12] S. Pokorski and L. Van Hove, *Acta Phys. Polon.* **B5** (1974) 229 and *Nucl. Phys.* **B86** (1975) 243; P. Carruthers, *Nucl. Phys.* **A418** (1984) 501c.
- [13] T.K. Gaisser and T. Stanev, *Phys. Lett.* **B219** (1989) 375.
- [14] T. Sjostrand and M. van Zijl, *Phys. Rev.* **D36** (1987) 2019.
- [15] X. N. Wang and M. Gyulassy, *Phys. Rev.* **D44** (1991) 3501; **D45** (1992) 844.
- [16] K. Geiger, *Phys. Rev.* **D46** (1992) 4965; **D46** (1992) 4986.
- [17] M. Gluck, E. Reya and A. Vogt, *Z. Phys.* **C67** (1995) 433 and references therein.
- [18] F.O. Durães, F.S. Navarra and G. Wilk, in preparation.
- [19] A. di Giacomo and H. Panagopoulos, *Phys. Lett.* **B285** (1992) 133.
- [20] Like studies of the energy flows in high energy hadronic and nuclear reactions and the inelasticity [10, 9], the phenomenon of the apparent limited number of sources in multiparticle distributions [21], leading charm production [11], the nuclear stopping power in relativistic heavy ion collisions [22], the effect of fluctuations in initial conditions for hydrodynamics [23] and the determination of the proton-proton and proton-air cross sections in cosmic rays [24].
- [21] R.M. Weiner, G. Wilk and Z. Włodarczyk, *Phys. Rev.* **D45** (1992) 2308.
- [22] Q.J. Liu, W.Q. Chao and G. Wilk, *Mod. Phys. Lett.* **A10** (1995) 1905.
- [23] *Fluctuation effects in initial conditions for hydrodynamics*, S. Paiva, Y. Hama and T. Kodama, to appear in *Phys. Rev.* **C**.
- [24] J. Bellandi, R.J. Covolan and A.L. Godoi, *Phys. Lett.* **B343** (1995) 410.

- [25] It can be also deflected with some invariant momentum transfer  $t$ . However, because the IGM does not include so far any transverse momentum transfers, the results presented here must be regarded as appropriately averaged/integrated over  $t$ .
- [26] As everywhere in the IGM ([7, 8, 9]) all masses are neglected here. This implies that our approach will be the more accurate the higher is the energy of the reaction and also that it will not be valid for very small values of  $M_X^2$ . The IGM is applicable (and was tested) from energies  $\sqrt{s} \geq 10$  GeV onward only and this value imposes a lower limit of applicability for the model.
- [27] Since already some time [28] the Pomeron is treated as being composed of partons, i.e., gluons and sea  $\bar{q}q$  pairs, in much the same way as hadrons, with some characteristic distribution functions which will presumably become accurately known in HERA experiments [29].
- [28] G. Ingelman and P. Schlein, *Phys. Lett.* **B152** (1985) 256; A. Donnachie and P. V. Landshoff, *Phys. Lett.* **B191** (1987) 309; *Nucl. Phys.* **B303** (1988) 634.
- [29] ZEUS Collaboration: M. Derrick et al., *Z. Phys.* **C68** (1995) 569 and references therein.
- [30] We could therefore (following A. Edin, G. Ingelman and J. Rathsman, *Phys. Lett.* **B366** (1996) 371 and references therein) avoid mentioning the name of Pomeron altogether and treat  $\mathcal{P}$  as a *preformed colour singlet* object consisting of only a part of the gluonic content of the diffractive proton which is then absorbed by the other proton.
- [31] B.R. Desai and U.P. Sukhatme, *Z. Phys.* **C24** (1984) 277.
- [32] V. Innocente et al., *Phys. Lett.* **B169** (1986) 285.
- [33] L. Lönnblad, *Z. Phys.* **C65** (1995) 285.
- [34] J.C. Collins et al., *Phys. Rev.* **D51** (1995) 3182.
- [35] M.G. Albrow et al., *Nucl. Phys.* **B108** (1976) 1.
- [36] P.J. Sutton, A.D. Martin, R.G. Roberts and W.J. Stirling, *Phys. Rev.* **D45** (1992) 2349.
- [37] H. Dijkstra et al., *Z. Phys.* **C31** (1986) 391.
- [38] M. Adamus et al., *Z. Phys.* **C39** (1988) 301.
- [39] K. Goulianos, *Phys. Lett.* **B358** (1995) 379 and references therein.
- [40] J. Bellandi, A.L. Godoi, R.J.M. Covolan and J. Montanha, "Diffractive Contribution to the Elasticity and to the Nucleonic Flux in the Atmosphere", Rockefeller University Report RU 96/E-07 (1996).
- [41] One should note that we have used in our fits a fair representation of DD data obtained by different groups at different energies and with different set-ups. Because the experimental definition of diffractive events changes from group to group these data are not necessarily consistent with each other. This fact is reflected in the obtained quality of our fits. The older FERMILAB (J. Schamberger et al., *Phys. Rev. Lett.* **34** (1975) 1121 and J.C. Armitage et al., *Nucl. Phys.* **B194** (1982) 365) and ISR (M.G. Albrow et al., *Nucl. Phys.* **B108** (1976) 1) data reporting approximate scaling (i.e.,  $1/M_X^2$  behaviour) may have some incompatibility with those in [4] and [5] above and they cover only relatively low values of  $M_X$ .
- [42] Cf., for example, Q.Q. Zhu, L.K. Ding, G.J. Wang and Y.D. He, *J. Phys.* **G20** (1994) 1383 and references therein. We plan to address this problem elsewhere.

## Figure Captions

**Fig. 1** IGM description of a proton-proton scattering : a) general case. b) with the formation of a diffractive system of invariant mass  $M_X$ .

**Fig. 2** a) Diffractive mass spectrum for  $pp$  collisions calculted with the IGM (eq.(14)) and compared with CERN-ISR data [35]. b) the same as a) with  $m_0 = 550$  MeV.

**Fig. 3** Diffractive mass spectrum for  $p\bar{p}$  collisions calculted with the IGM (eq.(14)) and compared with CERN-SPS Collider data [5].

**Fig. 4** Diffractive mass spectrum for  $p\bar{p}$  collisions calculted with the IGM (eq.(14)) and compared with FERMILAB Tevatron data [4].

**Fig. 5** a) Diffractive mass spectrum for  $p + \pi^+ \rightarrow p + X$  collisions calculted with the IGM (eq.(14)) and compared with experimental data [38]. b) The same as a) for  $p + K^+ \rightarrow p + X$  collisions.

**Fig. 6** a) Diffractive mass spectrum for  $\pi^+ + p \rightarrow \pi^+ + X$  collisions calculted with the IGM (eq.(14)) and compared with experimental data [38]. b) The same as a) for  $K^+ + p \rightarrow K^+ + X$  collisions.

**Fig. 7** a) Energy dependence of the function  $F(M_X^2, s)$  (16). b) Energy dependence of the function  $H(M_X^2, s)$  (17) calculted with the IGM.

**Fig. 8** a) Energy dependence of diffractive mass spectra calculated with the IGM (eq. (15)). The solid, dashed and dotted lines represent spectra at  $\sqrt{s} = 23.5, 44.6$  and  $62.4$  GeV respectively. b) The same as a) for  $\sqrt{s} = 0.54$  (solid lines),  $0.90$  (dashed lines) and  $1.8$  TeV (dotted lines). c) The same as a) for  $\sqrt{s} = 1.8$  (solid lines) and  $14$  TeV (dashed lines).

**Fig. 9** Energy dependence of the "diffractive inelasticity"  $\langle \xi \rangle$  and of  $\langle \xi^\varepsilon \rangle$ .

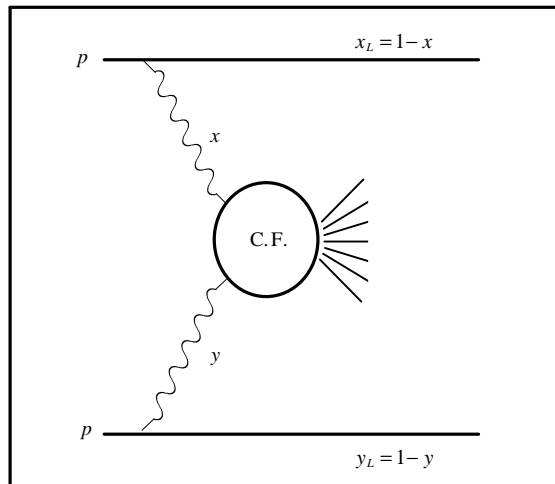


**Figure 1a**

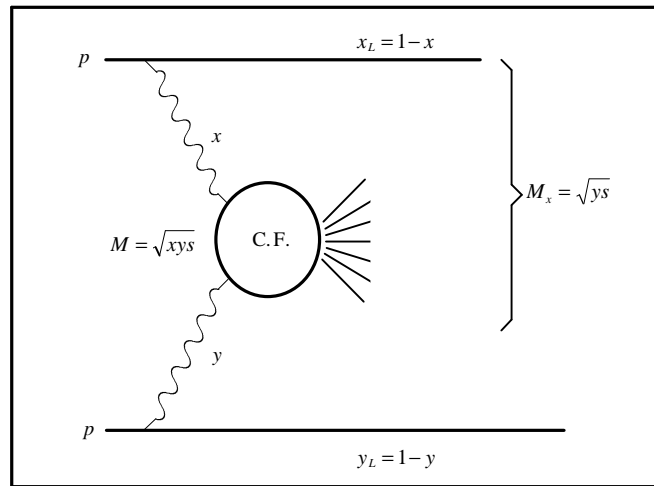


**Figure 1b**

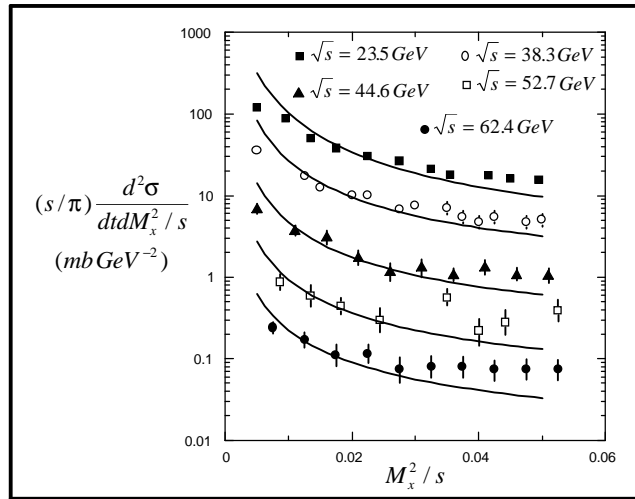


**Figure 2a**

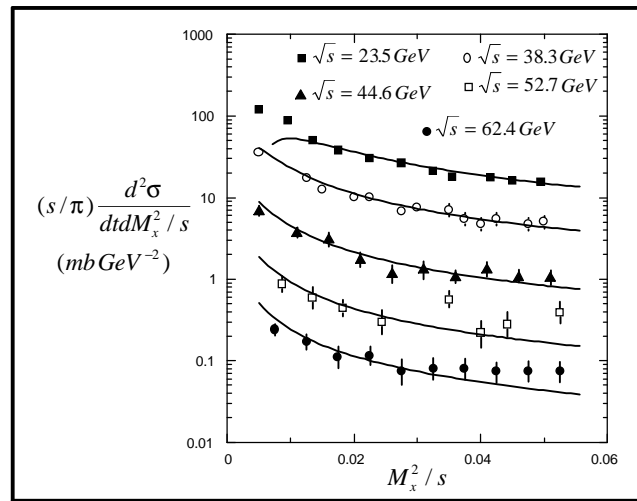


**Figure 2b**

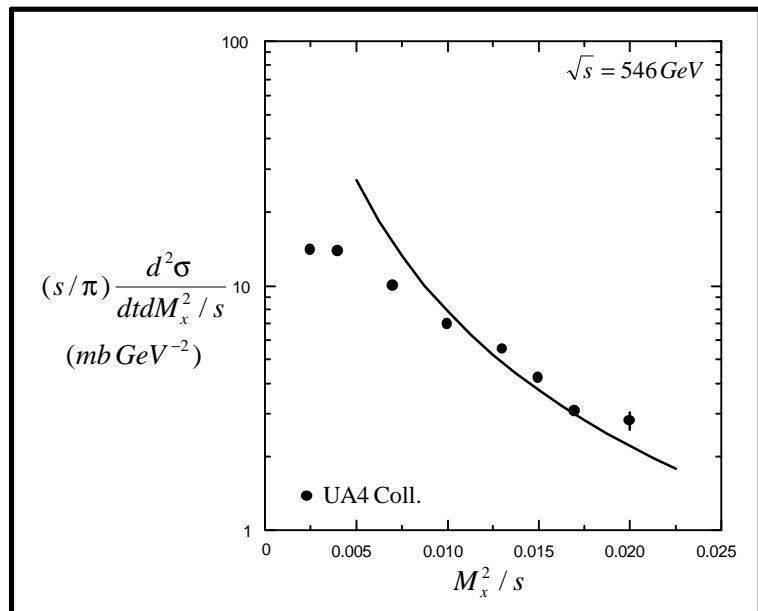


**Figure 3**

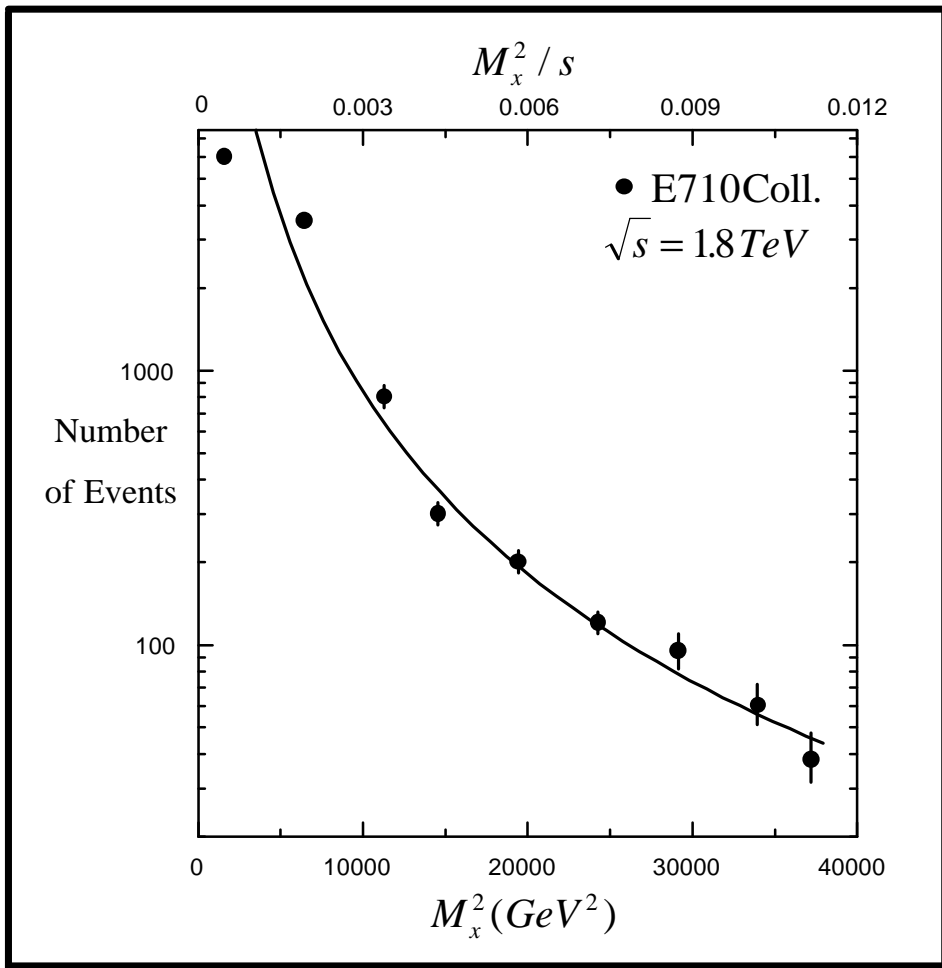


**Figure 4**

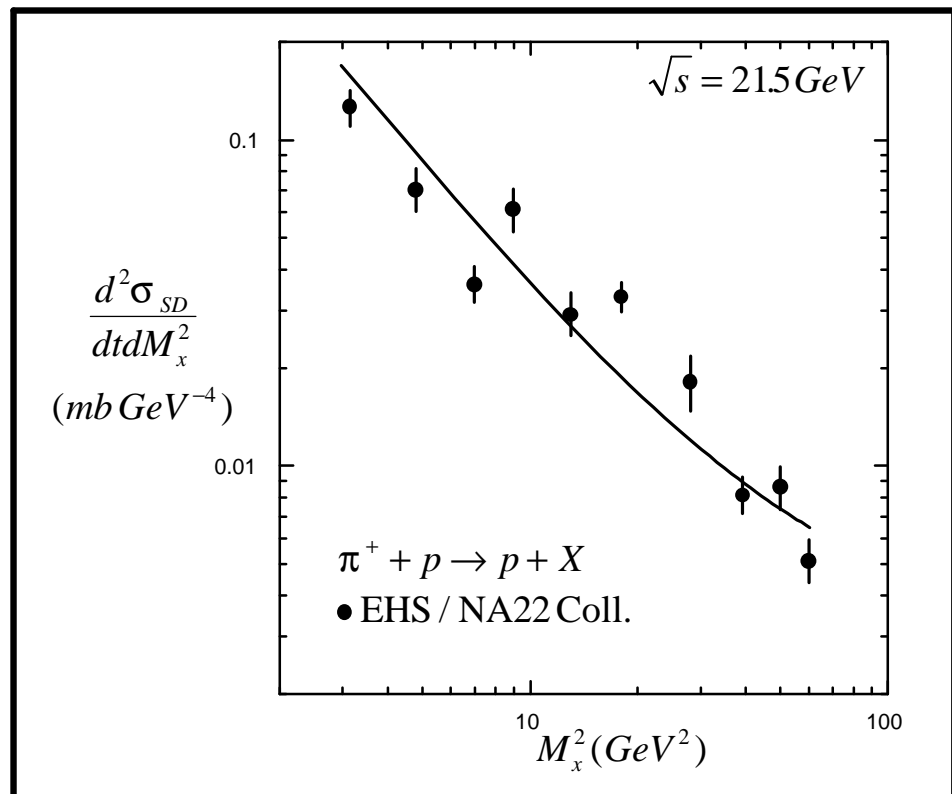


**Figure 5a**

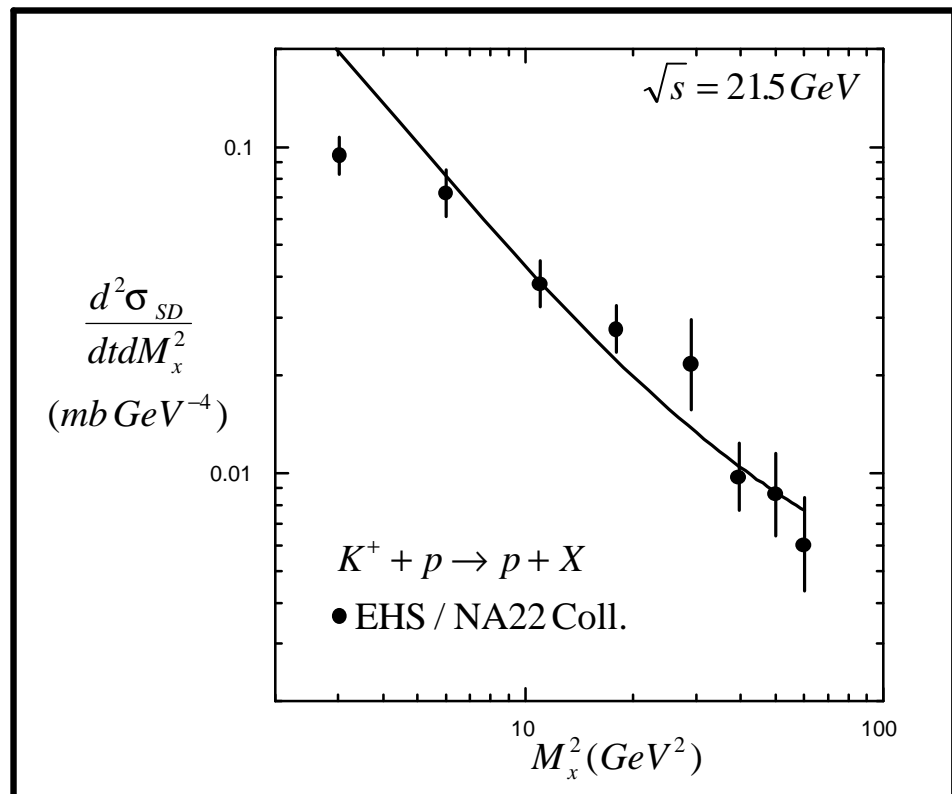


**Figure 5b**

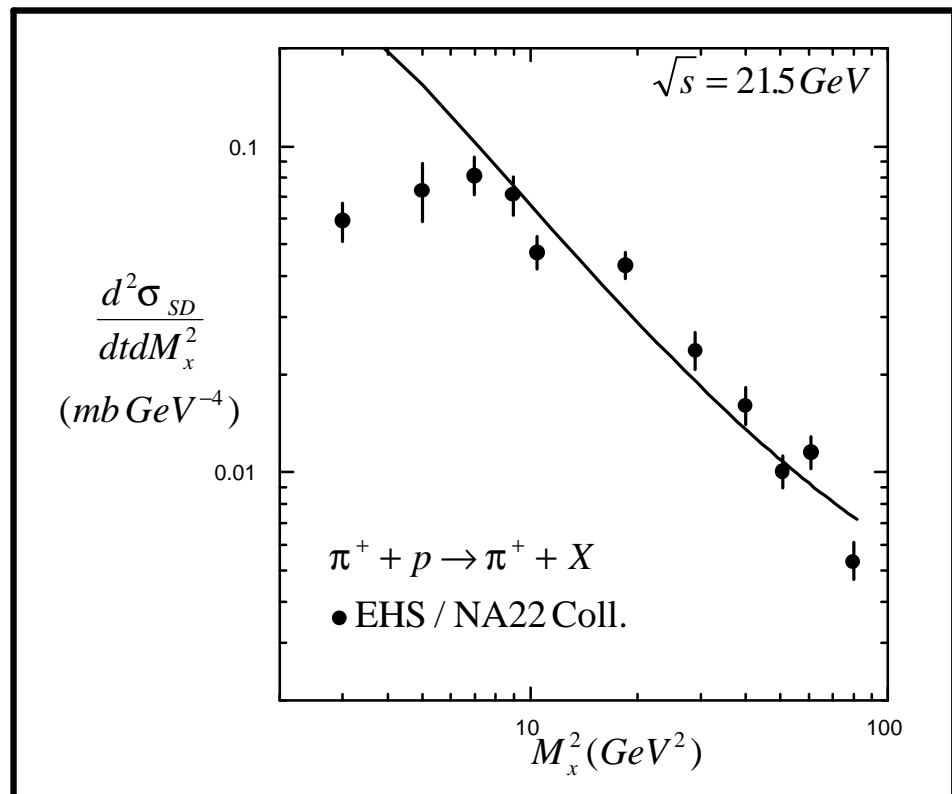


Figure 6a

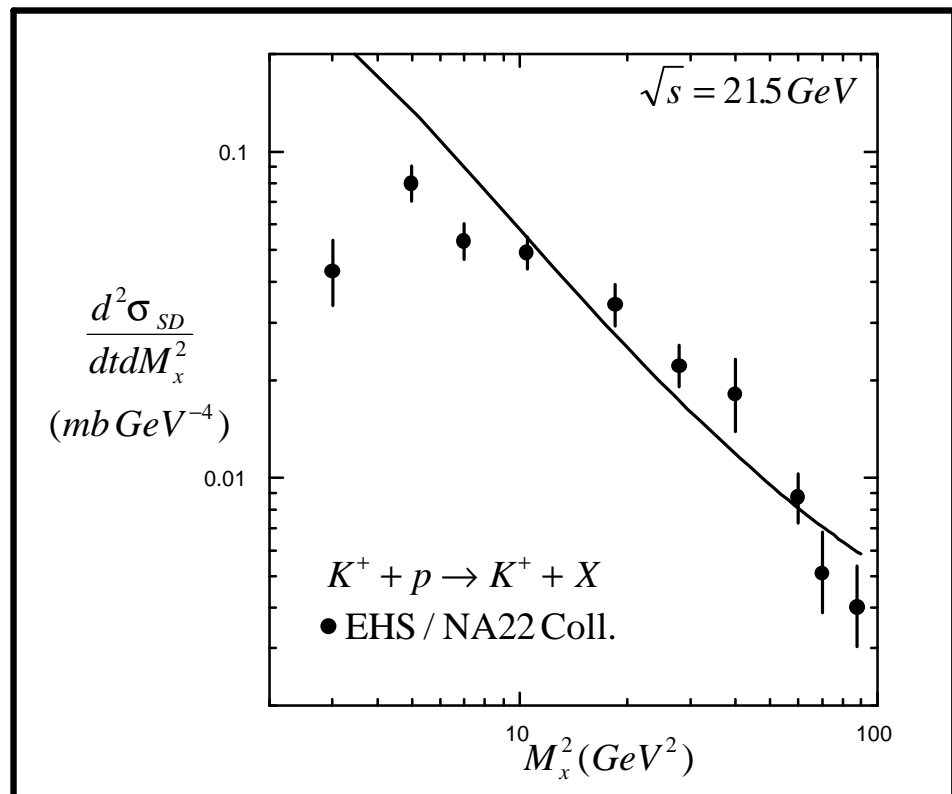
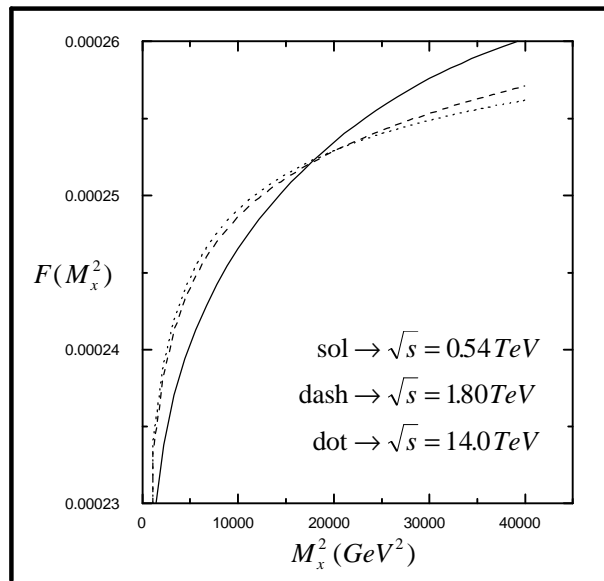
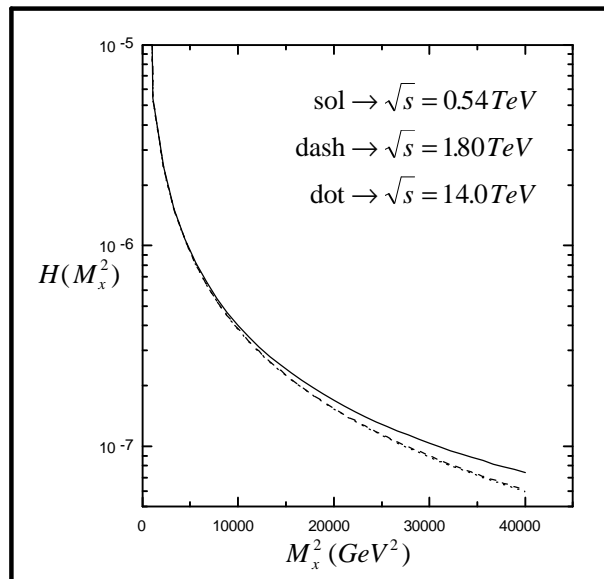


Figure 6b



**Figure 7a**



**Figure 7b**

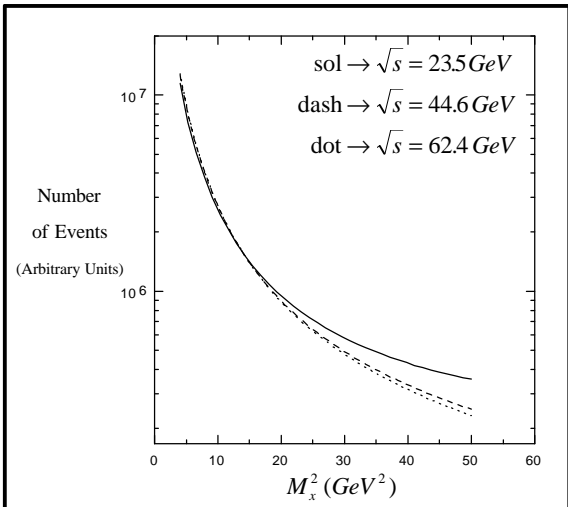


**Figure 8a**

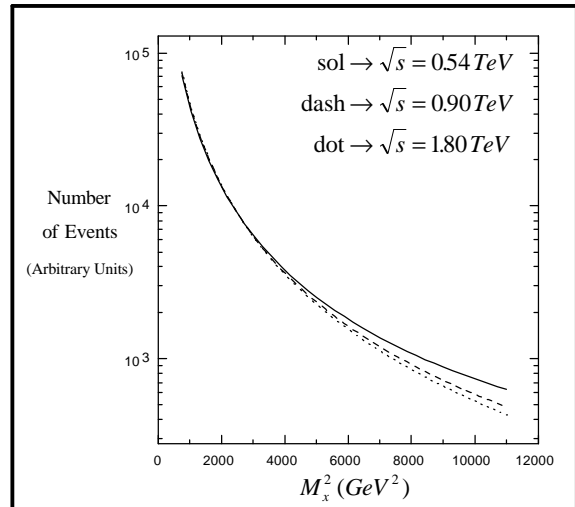


**Figure 8b**

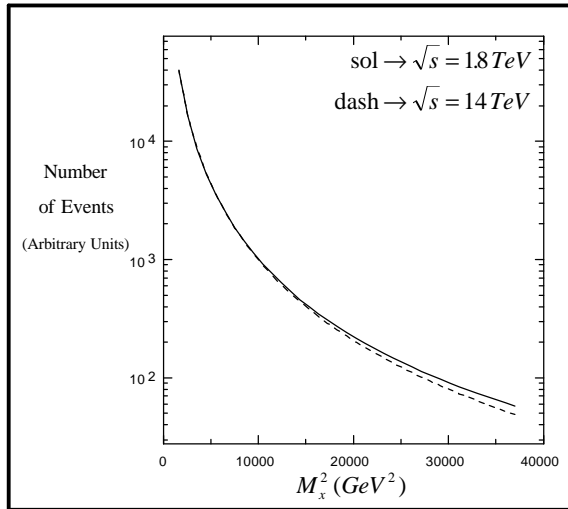


**Figure 8c**

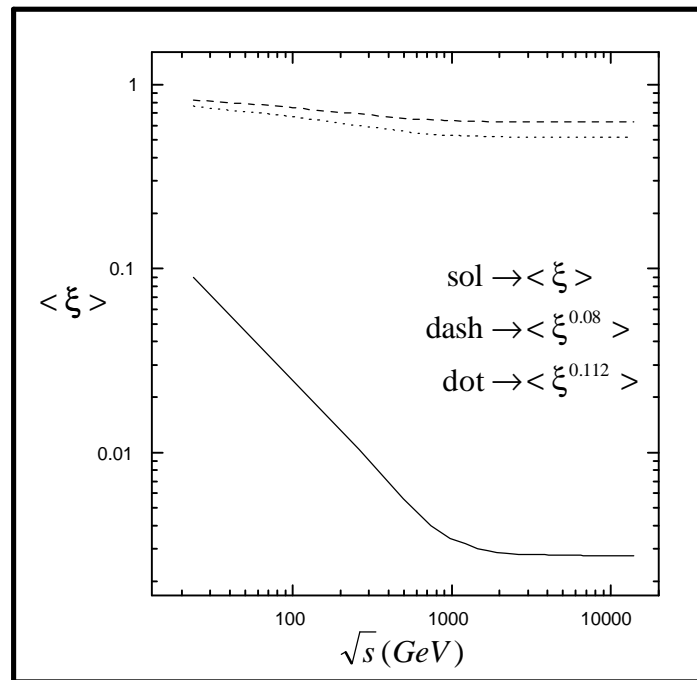


**Figure 9**